Multiple C-H···anion and N-H···anion Hydrogen Bond Directed Two-Dimensional Crystalline Nanosheet with Precise Distance Control of Surface Charges for Enhanced Capture DNA

Laicheng Zhou,[a, §] Ran He,[a, §] Yang Qin,[a] Yi-Lin Wu,[b] Li Jiang,[a] Dong-Dong Zhou,[a] and Ling Zhang[a]

Utilizing combined non-covalent interactions and introducing anions as structure-directing factors to build oriented self-assembly and 2D crystalline nanosheet superstructures with precise distance control of surface charges in competitive aqueous solvents still represents a formidable challenge for supramolecular chemists. Here, we report a simple, efficient, and general strategy for multiple C-H/N-H···anion hydrogen bond enhanced π–π interactions directed 2D oriented self-assembly in water, which is based on the head-to-tail association of perylene monoimide dimers (PMIs) by directing N−H−anion interactions position the anions to C-H of π systems (PMIs). Interesting, this behavior only occurs for the size-matched anions (Cl^- to NO_3^-; <45 $Å^3$), beyond which the larger anions could not form 2D crystalline nanosheet superstructures. The results showed that the crystalline nanosheet superstructures with precise distance control of surface charges could effectively capture DNA, possibly due to their high surface charge density and the distance match between the distance of surface charges and the distance between adjacent base pairs.

1 Introduction

Crafting of two-dimensional (2D) crystalline nanosheets with precise distance control of surface charges by 2D oriented self-assembly in aqueous solution is extremely important due to their potential applications in materials science and nanotechnology.[1] Oriented self-assembly and 2D crystalline nanosheet structures with precise distance control of surface charges seem to be rather common in nature. A key feature of nature's oriented self-assembly is that it could be based on combined non-covalent interactions in a biological and environmental media, which is known to be rich in numerous anions. Anions could play the important role in numerous biological and environmental processes, but anion involved in combined non-covalent interactions as structure-directing factors would be a real challenge, especially in water and biological media due to the intrinsic characteristics of anions. Anions have more diffuse charge in comparison with the corresponding isoelectronic cations, a large variety of geometries, and a greater dependence on the pH, and they are heavily solvated by polar solvents.[2] Only a few examples of the anion induced supramolecular polymers have been described.[3] Thus, introducing new strategy of combined non-covalent interactions and understanding anions as structure-directing factors to build oriented self-assembly and 2D crystalline nanosheet superstructures with precise distance control of surface charges in an aqueous solution for the materials and biological sciences are thus of interest for fundamental and practical reasons.

a PCFM Lab, and GDHPRC Lab, School of Chemistry, Sun Yat-Sen University, Guangzhou 510275, China. E-mail: ceszl@mail.sysu.edu.cn

b School of Chemistry, Cardiff University, Cardiff CF10 3AT, United Kingdom

§ These authors contributed equally to this work.

Some works about combined non-covalent interactions of synthetic molecular receptors had been reported for anion recognition and sensing. The dominant N−H functional groups and neutral and cationic C−H hydrogen bond donors could be directed toward the center of the macrocyclic cavity to position anions.[2] The directionality of interactions of electron-deficient π systems with spherical anions (e.g., halides) can be controlled by secondary effects such as N−H or C−H hydrogen bonding in organic solution phase.[4] Although multiple C-H/N-H···anion H-bonding (such as C_{sp^2}-H· · · anions, C_{sp^3}-H· · · anions and N-H· · · anions) interactions have been reported for the context of molecular self-assembly,[5] utilizing multiple C-H/N-H···anion H-bonding interactions as structure-directing factors for 2D crystalline nanosheets with precise distance control of surface charges in water has not yet been explored.

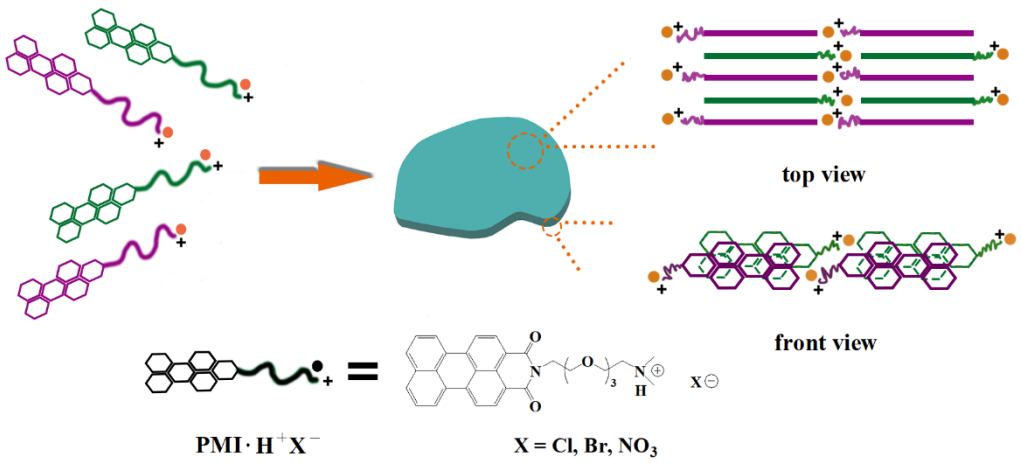

Scheme 1 Representation of the formation of supramolecular nanosheet structures by 2D oriented self-assembly for enhanced capture DNA. Top and front views of 2D sheet-like structures for PMI•H^+X^- (X^- = Cl^-, Br^- or NO_3^-).

Herein, we address this challenging issue and report a simple, efficient, and general strategy for an oriented self-assembly into 2D crystalline nanosheets with precise distance control of surface charges based on multiple C-H/N-H···anion H-bonding enhanced π–π interactions as structure-directing factors (Scheme 1). Although there are several reports on the regulation of foldamer-based receptor structures to bind anions using C_{sp^2}-H· · · anions hydrogen bonds,[6-10] this is the report of the utilization of multiple C-H/N-H···anion H-bonding (such as C_{sp^2}-H· · · anions, C_{sp^3}-H· · · anions and N-H· · · anions) interactions as structure-directing factors for 2D crystalline nanosheets with precise distance control of surface charges for enhanced capture DNA in an aqueous solution.

2 Results and discussion

We selected perylene monoimide (PMI), as chromophores for photocatalysis in supramolecular scaffolds based on pioneering works of Stupp group,[11-18] for providing a π moiety for $C_{sp}2$-H· · ·anion binding; *N*-functionalization with ethylene glycol hydrophilic linker to a *N,N*-dimethylamino head group can be protonated to afford NH···anion hydrogen bonding motif (see Figure S1). Compound PMIs dissolve in CH_2Cl_2 at room temperature but form a suspension in water. Anions, such as halide, carbonate and nitrate, were selected for their ubiquitousness in (physico)chemical sciences and are of the biological and therapeutic importance. With treatment of hydrochloric acid or hydrogen bromide, the compound PMIs dissolved in the aqueous solution to form a deep red solution. By introducing haloid acid into the solution, the N,N-dimethylamino species was gradually protonated by the acidic medium, leading to the formation of cations PMI•H^+X^- (X^- = Cl^- or Br^-), and a successive variation of the hydrophilic–hydrophobic balance and a better dissolution in water.

Interestingly, the introduction of halide anion could activate PMI (non-protonated monomers) to begin an unexpected lateral arrangement by oriented self-assembly into 2D crystalline nanosheet structures of PMI•H^+X^- (X^- = Cl^- or Br^-) (protonated monomers) in aqueous solution. Indeed, atomic force microscopy (AFM) revealed the presence of well-defined nanosheets with several hundred nanometres wide, approximately 0.83±0.05 nm height for PMI•H^+Cl^- and 0.94±0.05 nm height for PMI•H^+Br^-, respectively (Figure 1). The results strongly indicate the formation of single-layer sheets and the thickness of single-layer sheets determined by the width of an individual PMI molecule (~0.66 nm[18]), and that the slightly larger value observed may due to an adhered water layer or surface roughness. The high resolution-TEM (HR-TEM) images show that the sheets consist of parallel stripes that are straight over one hundred nanometers, and that distance between the stripes is ~3.4 Å (Figure 2a, b). Selected area electron diffraction patterns of PMI•H^+ Cl^- (Figure 2a inset) and PMI•H^+Br^- (Figure 2b inset) reveal bright and narrow rings, further confirm the crystalline nature of the sheets. Compared with PMI•H^+X^- (X^- = Cl^- or Br^-), non-protonated PMI controls are slightly soluble in water, and could not self-assemble to form the similar crystalline nanosheets observed by HRTEM. From these results, we inferred that the halide anion could play key roles in facilitating the oriented self-assembly into crystalline nanosheets.

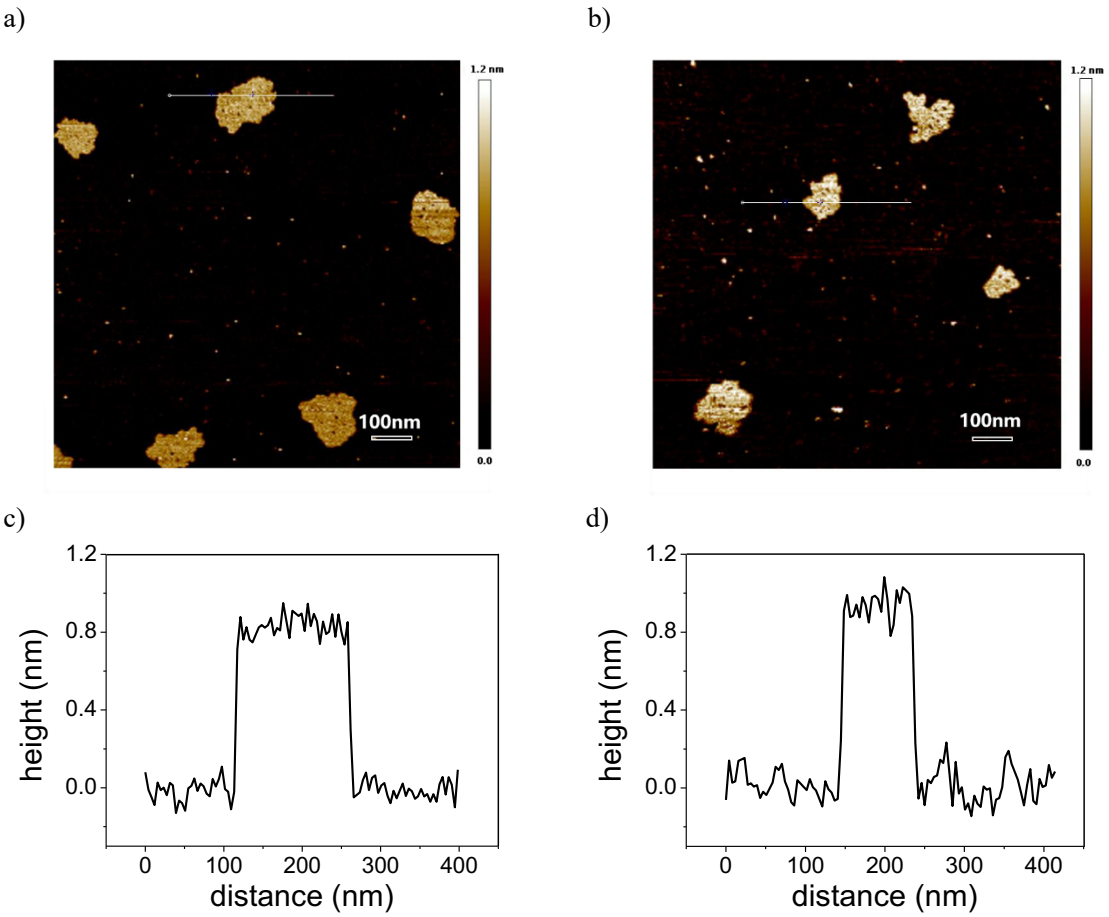

Fig. 1 AFM height mode image of 2D sheet-like structures for PMI•H^+Cl^- (a) and PMI•H^+Br^- (b) dilute aqueous solution (1.7× 10^{-4} M) dried onto freshly cleaved mica, respectively. c) Height line cut of AFM image in part a (white line). d) Height line cut of AFM image in part b (white line).

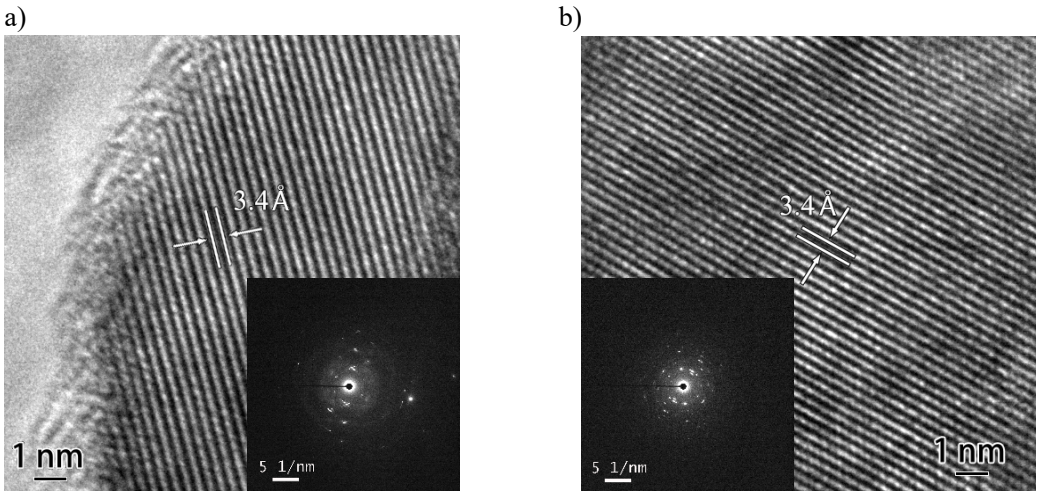

Fig. 2 HRTEM images of 2D sheet-like structures for PMI•H^+Cl^- (a) and PMI•H^+Br^- (b) dilute aqueous solution (1.7× 10^{-4} M), respectively. Scale bar: 1 nm. (Inset) SAED pattern from the corresponding PMI•H^+Cl^- (a) and PMI•H^+Br^- (b) systems, respectively.

To gain deeper insight into the 2D self-assembly of PMI•H^+X^-, crystals of PMI•H^+Br^- were grown in CH_3OH/Isopropyl ether (1:1, v/v) at room temperature and subject to X-ray

crystallography. Single-crystal X-ray analysis of PMI•H^+Br^- (Figure 3 and Figure S2) shows that bromide ions is hydrogen-bonded to the PMI's 9-postion H atom (C_{sp^2}-H··· Br^- has distances of 2.77 to 3.12 Å), strongly interacts with N-H (N···Br^- has distances of 3.13 to 3.57 Å) and also weakly interacts with the methyl and methylene H atoms of the cation (C_{sp^3}-H··· Br^- has distances of 2.96 to 3.76 Å). These interactions alongside electrostatic interaction of molecular dipole between anti-parallel PMIs dominate the crystal structure of PMI•H^+Br^- dimer. Single-crystal X-ray analysis of PMI•H^+Br^- confirmed the key roles of the halide anion for the 2D oriented self-assembly. Therefore, each PMI•H^+Br^- dimer in the crystal is stabilized by multiple H-bonding (C_{sp^2}-H· · · anions, C_{sp^3}-H· · · anions and N-H· · · anions) around bromide ions, coulombic interaction, dipolar interactions, and π–π stacking interactions of PMI rings. Powder X-ray diffraction (PXRD) were employed to provide a further evidence for the molecular arrangement of PMI•H^+ Br^- within the superstructures. By comparing characteristic diffraction peaks, measured and simulated PXRD patterns of PMI•H^+Br^- sample are almost identical (Figure S3), suggesting the same molecular packing within 2D oriented self-assembly.

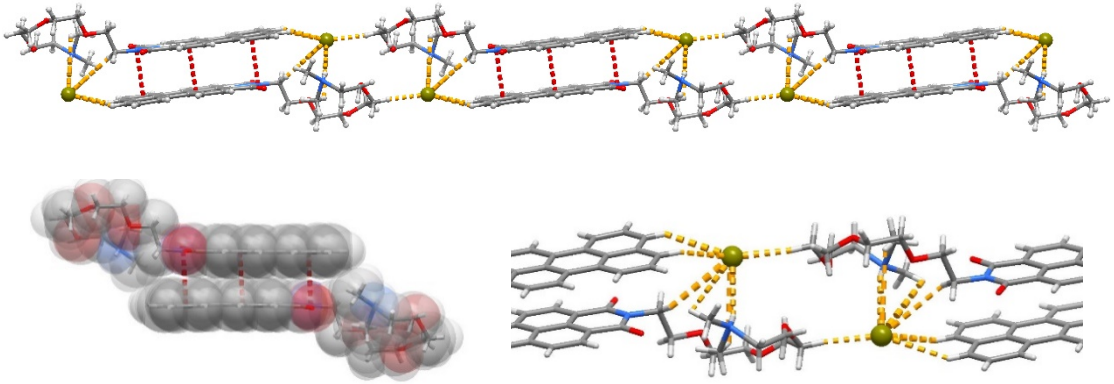

Fig. 3 X-ray crystal structure of the crystal packing of PMI•H^+Br^- viewed along the *a*-axis with the detailed hydrogen bonds and π-π intramolecular interactions. The software diamond 4 was used to construct the image from the crystallographic information files. Gray, carbon; white, hydrogen; blue, nitrogen; red, oxygen; chartreuse, bromide. Hydrogen bonds and π-π intramolecular interactions are shown as yellow and red dots.

The π-π intramolecular distance between anti-parallel PMI units in crystalline PMI•H^+Br^- of 3.3 Å (Figure 3) is well-matched to the measured stacking distance (3.4 Å) between the stripes from the HRTEM. These stripes can be attributed to the head-to-tail association of PMI•H^+Br^- dimers in one dimension. The stacking distance between the stripes corresponds to the π–π stacking distance of anti-parallel PMI core (plane-to-plane distance of π-stacked PMI), which permits the assembly of

the individual 1D stripes in the other dimension, leading to the formation of 2D crystalline sheets. Since these bi-functional PMI amphiphiles carry both the NH···X^- and aromatic functionalities, the cooperative multiple C-H/N-H··· halide anion H-bonding enhanced π–π interactions as structure-directing factors would drive the lateral arrangement of PMI layers by oriented self-assembly into 2D crystalline nanosheet structures in water.

Another measurement was to monitor the formation of 2D crystalline nanosheets driven by halide anion enhanced π–π interactions and to determinate association constant based on the change in nuclear magnetic resonance (NMR) spectra in D_2O over halide anion concentration (Figure 4). The ^{1}H NMR titration experiments were performed by adding tetrabutylammonium chloride (nBu$_4$NCl) and tetrabutylammonium bromine (nBu$_4$NBr) into D_2O solution of PMI•HBF_4, respectively. With the addition of halide anions (Cl^- or Br^-), the upfield shifts of all aromatic PMI protons (Figure 4a, 4b) indicate that the aggregates adopt a structure in which the anti-parallel PMI frameworks stack in a face-to-face geometry, as reported frequently in self-association phenomena arising from *π-π* stacking interactions. [7, 19-21] The chemical shifts upon complexation of Br^- were greater than those for Cl^-, which is attributed to the larger size of the halide, which exerts a steric pressure on the CH hydrogens. At the same time, the halide anion induced hydrogen bonds of the *N,N*-dimethylamino head groups (N-H · · ·halide anion) prefer to downfield shift of methyl protons (Figure 4c, 4d). Assuming 1:1 receptor/anion stoichiometry,[22] the association constant calculated by ^{1}H NMR spectroscopy in D_2O was modest (K_a ~ 29 M^{-1} for Cl^- and 88 M^{-1} for Br^-) (see Figure S4).

Based on the self-assembled PMI•H^+X^- (X^- = Cl^- or Br^-) systems driven by multiple C-H/N-H··· halide anion H-bonding enhanced π–π interactions, we can expect the PMI•H^+X^- (X^- = Cl^- or Br^-) to lose their individual excitonic character and behave as an ensemble in aqueous solution. The absorption maximum of PMI•H^+X^- (X^- = Cl^- or Br^-) in water blue shifted to 486 nm relative to the molecularly dissolved PMI•H^+X^- in DMSO ($\lambda_{max\ abs}$ = 500 nm) (see Figure S5). This hypsochromic shifts suggest the formation of face-to-face π–π stacking (the H-type aggregation) of the anti-parallel perylenes driven by multiple H-bonding interactions within the nanosheet systems. In emission, the red shift from λ_{em} = 553 nm in DMSO to λ_{em} = 574 nm in H_2O for PMI•H^+X^- (X^- = Cl^- or Br^-) and the decrease of emission intensity were also observed (see Figure S6). Non-protonated PMI controls are slightly soluble in water, resulting in the weak absorption signal and no emission signal (see Figure S7). Compared to non-protonated PMI controls, PMI•H^+X^- (X^- = Cl^- or Br^-) displayed a red

shift of $\Delta\lambda_{abs}$ = +10 nm in DMSO and $\Delta\lambda_{abs}$ = +69 nm in water. This increasing red-shifted absorption of PMI•H^+X^- (X^- = Cl^- or Br^-) in water indicated that this PMI•H^+Br^- nanosheet superstructure is more stabilized by multiple C-H/N-H···halide anion H-bonding enhanced π–π interactions in H_2O (a more polar solvent).

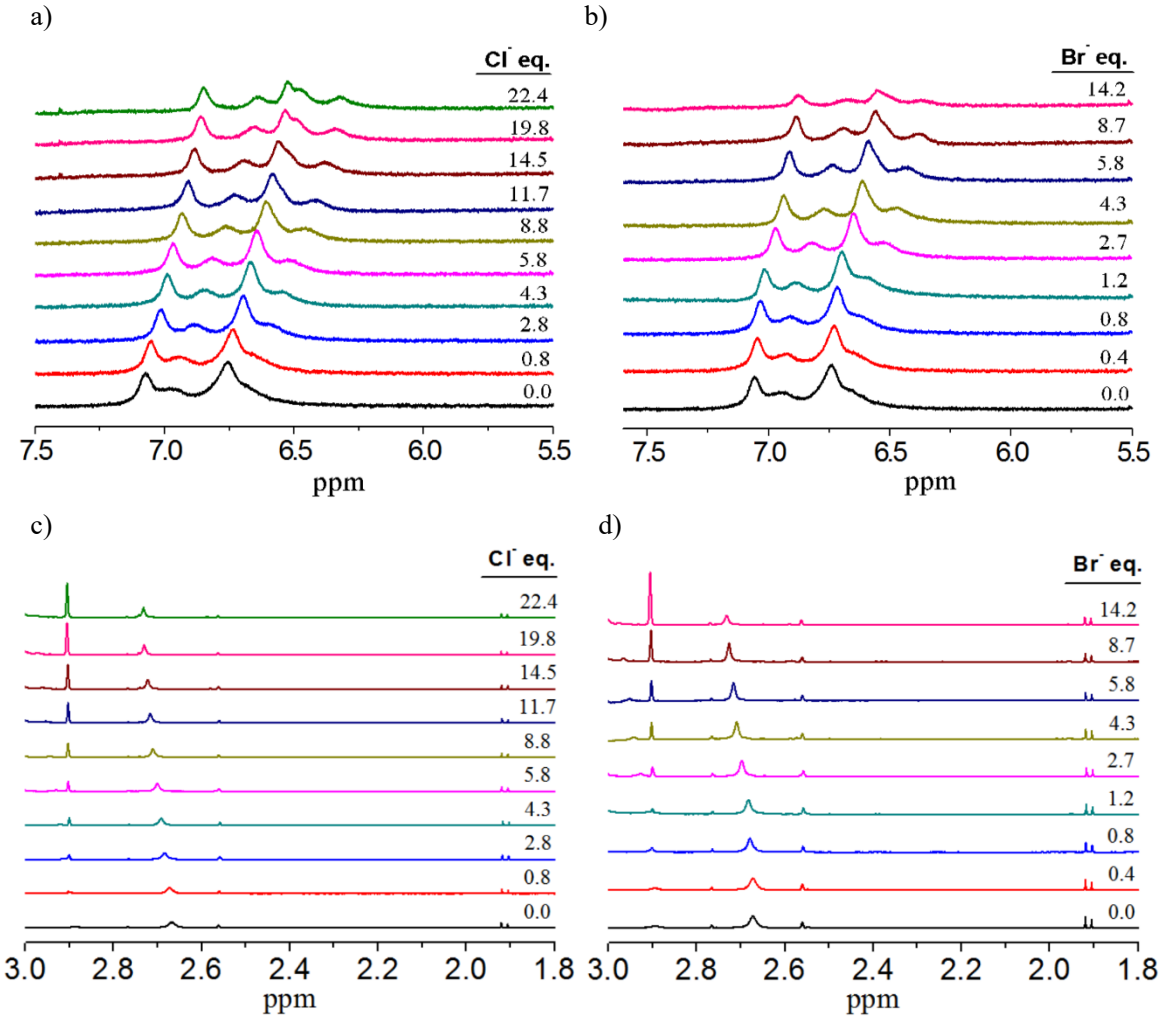

Fig. 4 Monitoring the formation of halide anion directed 2D crystalline nanosheets via the anion enhanced π–π interactions based on the change in the ^1H NMR spectrum of PMIs-HBF_4 in D_2O with the addition of different equiv of tetrabutylammonium chloride (a, c) and tetrabutylammonium bromine (b, d), respectively.

Considering the functional significance of trigonal planar nitrate anion, we selected nitrate (NO_3^-) anion with 41±1 $Å^3$ of spanning volume[10] to test 2D oriented self-assembly triggered by multiple C-H/N-H···nitrate anion H-bonding enhanced π–π interactions. With the introduction of the nitrate anions, the crystalline nanosheets by associating highly orientated 1D stripes could also be observed by HRTEM and SAED for PMI•$H^+NO_3^-$ system with a regular spacing of 3.4 Å (Figure 5). The result indicates the key role of nitrate anions is similar to that of halide anions for facilitating the 2D

oriented self-assembly. Despite the nitrate anion recognition based on combined non-covalent interactions,[3] this is the observation of crystalline nanosheets via nitrate anion-induced oriented self-assembly involved multiple C-H/N-H···nitrate anion H-bonding enhanced π–π interactions as structure-directing factors in water.

Based on above crystalline nanosheets by anion-induced oriented self-assembly, we wondered if crystalline nanosheets will expand to accommodate larger and larger anions (BF_4^-, ClO_4^- and HCO_3^-). No nanosheet with no electron diffraction dot of crystalline were observed for the larger anions (BF_4^- to ClO_4^-; >45 $Å^3$). Furthermore, we could not also observe the above 2D sheet-like structures by HRTEM when introducing CO_2-protonated head group of PMI, indicating the lack of multiple C-H/N-H···anion H-bonding around carbonate (HCO_3^-) does result in no formation of the similar 2D crystalline superstructure as those caused by halide anion. We believe the 2D oriented self-assembly is possible on the occasion when there are the strong multiple C-H/N-H···anion H-bonding interactions and complementary size matching between the anion and the cavity enclosed by three hydrophilic head groups.

a) b)

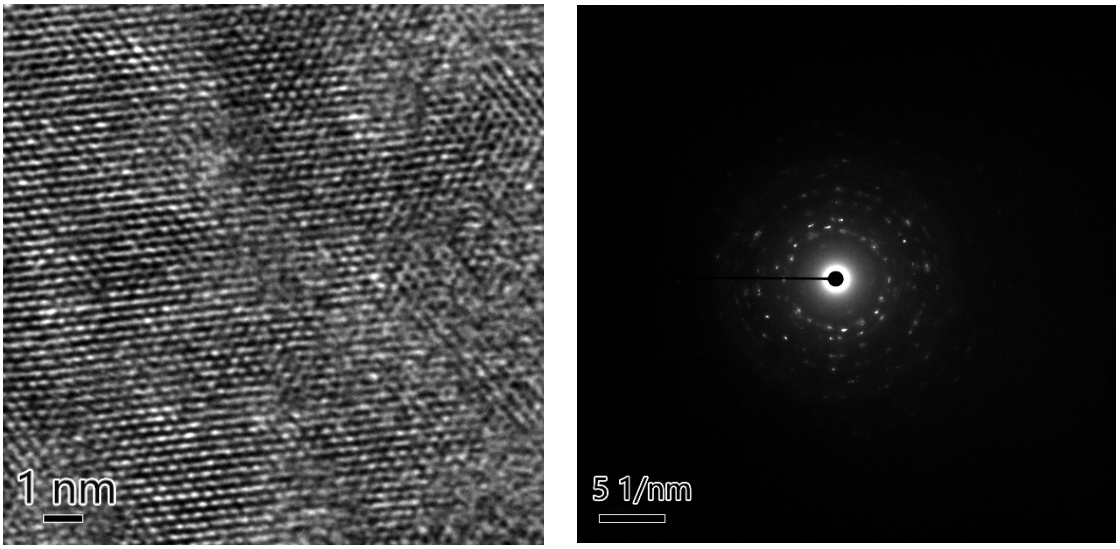

Fig. 5 (a) HRTEM image of 2D nanosheet-like structures for PMI•$H^+NO_3^-$ dilute aqueous solution (1.7×10^{-4}M). Scale bar: 1 nm. (b) SAED pattern from the corresponding PMI•H^+ NO_3^- nanosheet system.

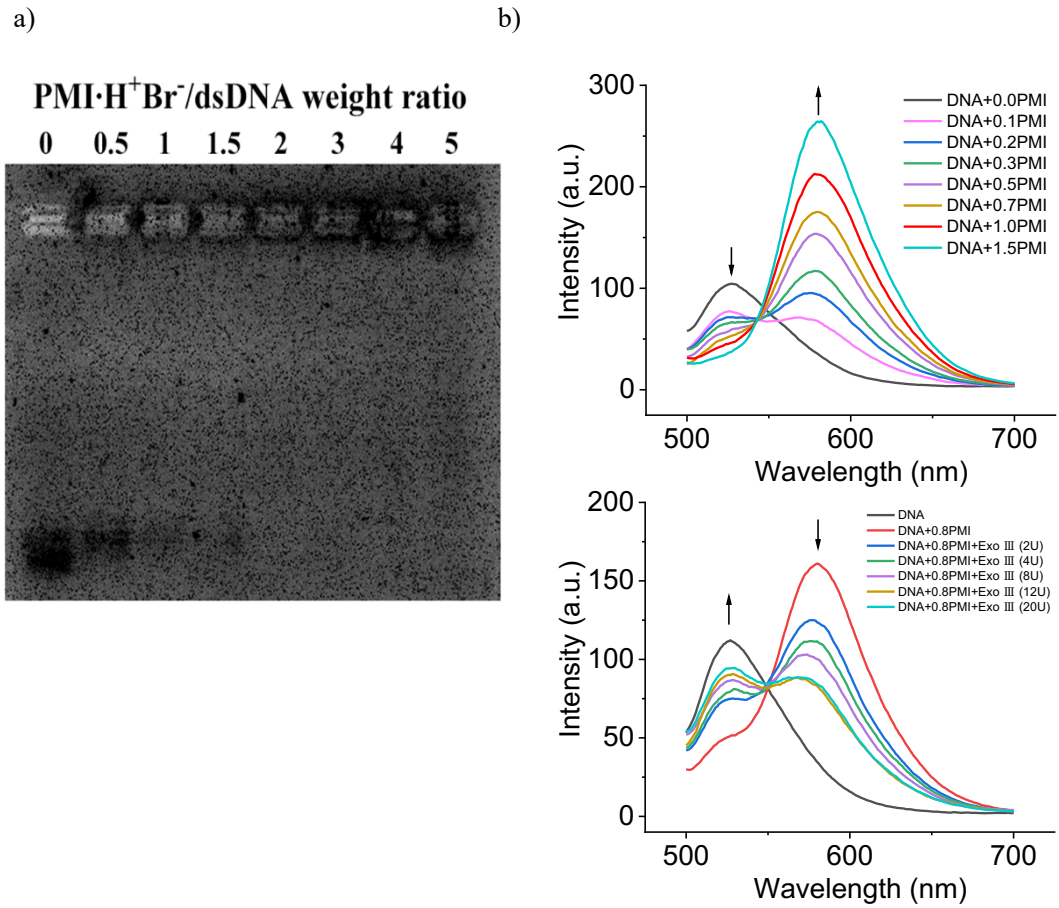

Fig. 6 (a) Agarose gel electrophoresis of the PMI•H$^+$Br$^-$/dsDNA complex with various ratios of the PMI•H$^+$Br$^-$ conjugate to dsDNA. (b) Fluorescence spectra of the PMI•H$^+$Br$^-$/dsDNA complex with various ratios of the PMI•H$^+$Br$^-$ conjugate to dsDNA (up), and Fluorescence spectra of different amounts of Exo III in DNA cleavage experiment (λ_{ex} = 485 nm) (down).

We demonstrate by a simple model that anions play a structural role for oriented self-assembly and that anion adsorption sites located on the surface of the crystalline nanosheets are responsible for this precise distance control of surface charges. Single-crystal x-ray analysis of PMI•H$^+$Br$^-$ shows that the distance of surface charges is dependent on the estimate of the length of an individual PMI molecule (~8.8 Å) and on π–π stacking distance (~3.4 Å), which is well matched with the distance between adjacent base pairs of DNA (~3.4 Å). The capture DNA of PMI•H$^+$Br$^-$ nanosheets by the electrostatic interaction between negatively charged DNA and the positively charged PMI•H$^+$Br$^-$ nanosheet were assessed by agarose gel electrophoresis and by energy transfer from the FAM to PMI•H$^+$Br$^-$ nanosheets (Fig. 6). As Fig. 6a shown, the PMI•H$^+$Br$^-$/dsDNA complex appeared to be formed when the weight ratio of the PMI•H$^+$Br$^-$ conjugate to dsDNA was very low (>1), due to the extremely high surface charge density of nanosheets. Upon increasing mass ratio of PMI•H$^+$Br$^-$/FAM-labeled dsDNA from 0 to 1.5, energy transfer due to the mechanism of Förster Resonance Energy Transfer (FRET) from FAM (emission peak at 526 nm) to PMI•H$^+$Br$^-$ nanosheets

would lead to quenching of FAM fluorescence (Fig. 6b up). In the presence of Exo III for DNA cleavage experiment, the cleavage would then turn the FRET "off", leading to a recovery of FAM fluorescence (Fig. 6b down). The increase of FAM emission and the decrease of the emission of PMI•H^+Br^- nanosheets with the increase of Exo III amounts in DNA cleavage experiment could further demonstrate the presence of the FRET mechanism of energy transfer. These results indicated that the crystalline nanosheet superstructures with precise distance control of surface charges could effectively capture DNA, possibly due to their high surface charge density and the distance match between the distance of surface charges and the distance between adjacent base pairs. Furthermore, the crystalline nanosheet superstructures with precise distance control of surface charges could provide a platform for the detection of biomoleculars (such as DNA, enzymes) based on the FRET "on" or "off".

3 Conclusions

In conclusion, we demonstrate this approach can be applied as a general design strategy for the synthesis of 2D crystalline sheet-like structures with precise distance control of surface charges by oriented self-assembly driven by multiple C-H/N-H···anion H-bonding (C_{sp^2}-H· · · anions, C_{sp^3}-H· · · anions and N-H· · · anions) enhanced π–π interactions. The present finding opens a new avenue toward directing functional molecular units to assemble into a highly oriented 2D crystalline structure with precise distance control of surface charges driven by the cooperative combination of π–π interactions, molecular dipolar interactions and multiple C-H/N-H···anion H-bonding interactions, which could provide the promise of novel properties that emerge from their unique topology and structural precision, and an as-yet undeveloped application space.

Conflicts of interest

There are no interests to declare.

Acknowledgements

This research was supported by the program of National Natural Science Foundation of China (Grant 21374137), Science and Technology Program of Guangzhou (Grant 201804010017), Natural Science Foundation of Guangdong province (Grant 2014A030313194), and Science and Technology Program of Guangdong province (Grant 2017A050506021). The authors gratefully acknowledge Prof. Kelong Zhu for helpful discussion, and Li Gong for the AFM measurements. We thank the staff of BL17B beamline at the Shanghai Synchrotron Radiation Facility, Shanghai, People's Republic of China, for assistance during data collection.

Notes and references

1 (*a*) M. Q. Zeng, Y. Xiao, J. X. Liu, K. N. Yang and L. Fu, *Chem. Rev.*, 2018, **118**, 6236–6296; (*b*) C. L. Tan, X. H. Cao, X. J. Wu, Q.Y. He, J. Yang, X. Zhang, J. Z. Chen, W. Zhao, S. K. Han, G. H. Nam, M. Sindoro and H. Zhang, *Chem. Rev.*, 2017, **117**, 6225–6331.

2 P. Molina, F. Zapata and A. Caballero, *Chem. Rev.,* 2017, **117**, 9907−9972.

3 (*a*) Q. He, P. Y. Tu and J. L. Sessler, *Chem,* 2018, **4**, 46−93; (*b*) F. Zapata, L. González, A. Bastida, D. Bautista and A. Caballero, *Chem. Commun.,* 2020, **56**, 7084−7087; (*c*) H. Y. Gong, B. M. Rambo, E. Karnas, V. M. Lynch and J. L. Sessler, *Nat. Chem.,* 2010, **2**, 406−409; (*d*) F. Zapata, L. González, A. Caballero, A. Bastida, D. Bautista and P. Molina, *J. Am. Chem. Soc.,* 2018, **140**, 2041−2045; (*e*) P. Sabater, F. Zapata, A. Bastida and A. Caballero, *Org. Biomol. Chem.,* 2020, **18**, 3858−3866.

4 (*a*) M. Müller, M. Albrecht, V. Gossen, T. Peters, A. Hoffmann, G. Raabe, A. Valkonen and K. Rissanen, *Chem. - Eur. J.,* 2010, **16**, 12446−12453; (*b*) A. Bretschneider, D. M. Andrada, S. Dechert, S. Meyer, R. A. Mata and F. Meyer, *Chem. - Eur. J.,* 2013, **19**, 16988−17000.

5 (*a*) N. Barooah, A. Karmakar, R. J. Sarma and J. B. Baruah, *Inorg. Chem. Commun.,* 2006, **9**, 1251−1254; (*b*) J. C. Tenorio, R. S. Corrêa, A. A. Batista and J. Ellena, *J. Mol. Struct*., 2013, **1048**, 274−281.

6 Y. R. Hua and A. H. Flood, *J. Am. Chem. Soc.,* 2010, **132**, 12838−12840.

7 Y. L. Li and A. H. Flood, *J. Am. Chem. Soc.,* 2008, **130**, 12111−12122.

8 Y. R. Hua, Y. Liu, C. H. Chen and A. H. Flood, *J. Am. Chem. Soc.,* 2013, **135**, 14401−14412.

9 Y. Liu, F. C. Parks, W. Zhao and A. H. Flood, *J. Am. Chem. Soc.,* 2018, **140**, 15477−15486.

10 F. C. Parks, Y. Liu, S. Debnath, S. R. Stutsman, K. Raghavachari and A. H. Flood, *J. Am. Chem. Soc.,* 2018, **140**, 17711−17723.

11 A. S. Weingarten, R. V. Kazantsev, L. C. Palmer, M. McClendon, A. R. Koltonow, A. P. S. Samuel, D. J. Kiebala, M. R. Wasielewski and S. I. Stupp, *Nat. Chem.,* 2014, **6**, 964-970.

12 A. S. Weingarten, R. V. Kazantsev, L. C. Palmer, D. J. Fairfield, A. R. Koltonow and S. I. Stupp, *J. Am. Chem. Soc*., 2015, **137**, 15241-15246.

13 N. J. Hestand, R. V. Kazantsev, A. S. Weingarten, L. C. Palmer, S. I. Stupp and F. C. Spano, *J. Am. Chem. Soc.,* 2016, **138**, 11762-11774.

14 R. V. Kazantsev, A. J. Dannenhoffer, T. Aytun, B. Harutyunyan, D. J. Fairfield, M. J. Bedzyk and S. I. Stupp, *Chem,* 2018, **4**, 1596-1608.

15 R. V. Kazantsev, A. J. Dannenhoffer, A. S. Weingarten, B. T. Phelan, B. Harutyunyan, T. Aytun, A. Narayanan, D. J. Fairfield, J. Boekhoven, H. Sai, A. Senesi, P. I. O'Dogherty, L. C. Palmer, M. J. Bedzyk, M. R. Wasielewski and S. I. Stupp, *J. Am. Chem. Soc.,* 2017, **139**, 6120-6127.

16 F. Tantakitti, J. Boekhoven, X. Wang, R. V. Kazantsev, T. Yu, J. Li, E. Zhuang, R. Zandi, J. H. Ortony, C. J. Newcomb, L. C. Palmer, G. S. Shekhawat, M. O. de la Cruz, G. C. Schatz and S. I. Stupp, *Nat. Mater.,* 2016, **15**, 469-476.

17 A. S. Weingarten, A. J. Dannenhoffer, R. V. Kazantsev, H. Sai, D. Huang and S. I. Stupp, *J. Am. Chem. Soc.,* 2018, **140**, 4965-4968.

18 B. Harutyunyan, A. Dannenhoffer, S. Kewalramani, T. Aytun, D. J. Fairfield, S. I. Stupp and M. J. Bedzyk, *J. Phys. Chem. C,* 2017, **121**, 1047−1054.

19 S. L. Lahiri, J. L. Thompson and J. S. Moore, *J. Am. Chem. Soc.,* 2000, **122**, 11315–11319.

20 S. Höger, K. Bonrad, A. Mourran, U. Beginn and M. Möller, *J. Am. Chem. Soc.,* 2001, **123**, 5651–5659.

21 R. B. Martin, *Chem. Rev.,* 1996, **96**, 3043–3064.

22 (*a*) A. Bretschneider, D. M. Andrada, S. Dechert, S. Meyer, R. A. Mata and F. Meyer, *Chem. - Eur. J.* 2013, **19**, 16988−17000; (*b*) Y. S. Rosokha, S. V. Lindeman, S. V. Rosokha and J. K. Kochi, *Angew. Chem. Int. Ed.* 2004, **43**, 4650–4652.